On the Dynamics of Charging in Nanoporous Carbon-Based Supercapacitors

Clarisse Péan,[†,‡,§] Céline Merlet,[†,§] Benjamin Rotenberg,[†,§] Paul Anthony Madden,[⊥] Pierre-Louis Taberna,[‡,§] Barbara Daffos,[‡,§] Mathieu Salanne,[†,§,*] and Patrice Simon[‡,§]

[†]Sorbonne Universités, UPMC Univ Paris 06, UMR 8234, PHENIX, F-75005 Paris, France, [‡]CIRIMAT, UMR CNRS 5085, Université Paul Sabatier, Bat. 2R1, 118 route de Narbonne, 31062, Toulouse Cedex 9, France, [§]Réseau sur le Stockage Electrochimique de l'Energie (RS2E), FR CNRS 3459, 80039 Amiens Cedex, France, and [⊥]Department of Materials, University of Oxford, Parks Road, Oxford OX1 3PH, United Kingdom

ABSTRACT Supercapacitors are electricity storage systems with high power performances. Their short charge/discharge times are due to fast adsorption/desorption rates for the ions of the electrolyte on the electrode surface. Nanoporous carbon electrodes, which give larger capacitances than simpler geometries, might be expected to show poorer power performances because of the longer times taken by the ions to access the electrode interior. Experiments do not show such trends, however, and this remains to be explained at the molecular scale. Here we show that carbide-derived carbons exhibit heterogeneous and fast charging dynamics. We perform molecular dynamics simulations, with realistically modeled nanoporous electrodes and an ionic liquid electrolyte, in which the system, originally at equilibrium in the uncharged state, is suddenly perturbed by the application of an electric potential difference between the electrodes. The electrodes respond by charging progressively from the interface to the bulk as ions are exchanged between the nanopores and the electrolyte region. The simulation results are then injected into an equivalent circuit model, which allows us to calculate charging times for macroscopic-scale devices.

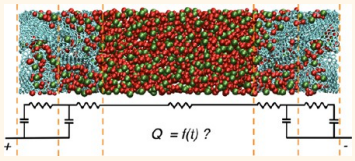

KEYWORDS: supercapacitor · room temperature ionic liquid · nanoporous carbon · molecular dynamics · power density · transmission line model

Supercapacitors are currently used in specific applications for which high power is required for a short time.[1] The electricity storage is achieved by (non-faradaic) adsorption of ions from an electrolyte onto electrodes with high-surface area; this surface-based mechanism, which involves no redox reaction, is at the origin of high power.[2,3] As devices, supercapacitors complement batteries, which have slower discharge time but which exhibit much greater stored energy densities.[4] Many applications therefore use this complementarity and combine a supercapacitor with a Li-ion battery. Nevertheless, there is a tremendous need to increase the stored energy densities of supercapacitors, and various routes are currently explored.[5−10] Recent advances were made when it was shown that using electrodes made of carbons with well-controlled nanoporosity could lead to large and unexpected enhancements of the capacitance.[11−13] However, these improvements must be made while keeping good power performance.

Energy density is proportional to the capacitance, which is an equilibrium property. So far most of the simulation studies were dedicated to the understanding of the origin of the "anomalous" increase of the capacitance inside nanoporous carbon electrodes,[14−21] without addressing the dynamic aspects. Nevertheless, it is the transport of the ions inside the pores which will control the power density of a device. It is thus of primary importance to well characterize this transport on the molecular scale. A few studies have investigated the relaxation dynamics of ions close to electrified planar surfaces.[22−24] In a study directed at the nanoporous carbons, Kondrat and Kornyshev have recently observed by using a mean-field model that the charging of initially empty pores proceeds in a front-like way, while that of already filled pores is diffusive.[25]

There are two main methods for modeling the electrodes of a supercapacitors. The first, simpler one consists in assigning constant charges to every atom of an electrode, while the second one consists in applying a constant potential and allowing the carbon charges to fluctuate in response to the local

* Address correspondence to mathieu.salanne@upmc.fr.

Received for review November 10, 2013 and accepted January 13, 2014.

Published online January 13, 2014
10.1021/nn4058243

© 2014 American Chemical Society

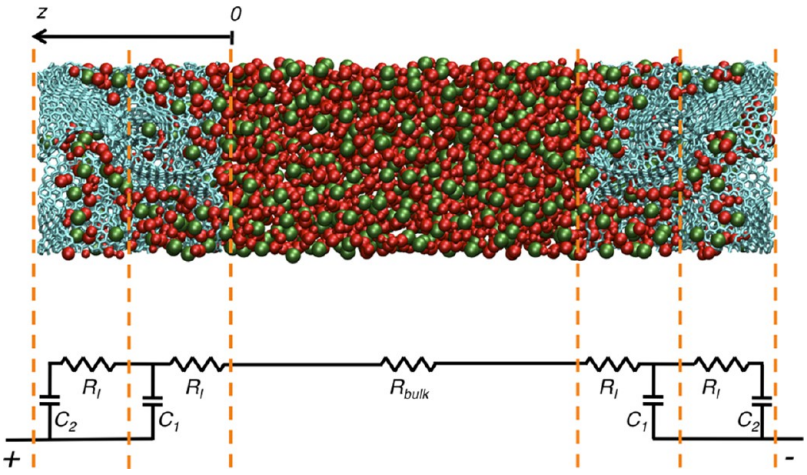

Figure 1. (Top) The simulation cell consists of a BMI-PF_6 ionic liquid electrolyte surrounded by two porous electrodes (CDC-1200) held at constant electrical potentials (blue, C atoms; red, the three sites of BMI^+; and green, PF_6^- ions). (Bottom) Equivalent electric circuit used to model our simulation setup. R_{bulk} is the resistance of the electrolyte in the bulk region, R_l is the resistance of the electrolyte adsorbed in an electrode slice, C_1 and C_2 are the capacitances of the two slices.

structure of the electrolyte.[26−28] It was shown that the latter approach is much more realistic, and should always be used when studying the dynamics. Constant charge simulations should be kept for equilibration purposes only, because imposing a sudden surface charge leads to an extremely large current at $t = 0$, and consequently to unphysically fast dynamics and a large increase of the temperature of the system.[29] Here we perform *constant potential* molecular dynamics simulations involving realistic models of nanoporous carbon electrodes with an ionic liquid electrolyte. We study the response of the supercapacitors to a suddenly applied electrical potential difference. We show that the charge penetrates progressively from the carbon/electrolyte interface to the bulk of the electrodes. The charging dynamics is, however, markedly heterogeneous at the nanoscale. Finally, by using an equivalent circuit model, we show that a macroscopic electrode would charge on the time scale of 1 s, which means that the power density of such a device would be very good.

RESULTS AND DISCUSSION

Charging Dynamics. The system we simulate is composed of an ionic liquid electrolyte (1-butyl-3-methylimidazolium hexafluorophosphate, BMI-PF_6) confined between a pair of nanoporous carbon electrodes, as shown on Figure 1. For the latter, three structures which were obtained by Palmer *et al.* by performing quenched molecular dynamics at various thermal rates[30] were used. They were shown to mimic very well carbide-derived carbons (CDCs)[31] obtained under various synthesis temperatures, so that we will label them following the corresponding temperatures in °C: CDC-800, CDC-950, and CDC-1200. They differ mostly by their local nanoporosity (pore sizes and shapes). In particular, their respective average pore sizes are 7.5, 9.0, and 9.0 Å (with distributions ranging from 3 to 15−18 Å).[30] In addition, the structure becomes more and more disordered when passing from CDC-1200 to CDC-950 and then to CDC-800. Here after equilibration of the system at 0 V, we suddenly apply an electric potential difference (a value of 1 V was used unless otherwise stated) and follow the charging dynamics of the electrodes.

We have previously studied[18,28] the equilibrium aspects of the adsorption of ions in these systems over a range of applied potentials. Even at zero applied potential, this electrolyte is found to wet the pores of the carbon electrodes effectively such that equal numbers of cations and anions are absorbed within the nanopores. When a potential is applied, there is an exchange of ions between the bulk electrolyte and those absorbed within the electrode interiors such that, after equilibration, there is a net excess of cations within the electrode held at negative potential and the electrode develops a net charge which balances the excess charge of the absorbed ions.[16,18,32] To a good approximation, the total volume of electrolyte within the electrode is not affected by the application of a potential.

Figure 2 shows the time evolution of the average charge per carbon inside the positive electrode for each of the three different porous materials studied after the potential difference is applied between the electrodes. They all reach a plateau value of ≈0.007 e/carbon atom for CDC-1200 and CDC-950 and of ≈0.006 e/carbon atom for CDC-800. It is probable that the fully charged régime is not reached on the time scale of these simulations: for example, in CDC-1200, we expect to reach a maximal charge of ≈0.011 e/carbon atom which is obtained in calculations where we allow sufficient time for full equilibration.[18] This observation is consistent with an experimental observation that the

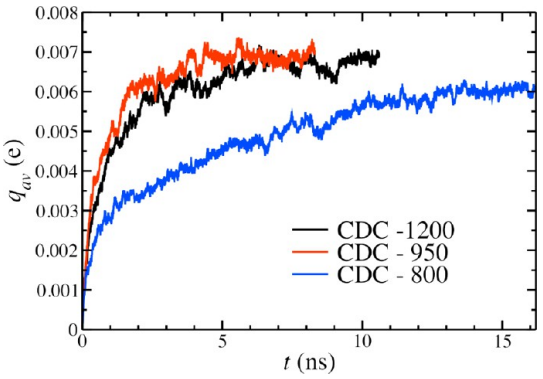

Figure 2. Time evolution of the average charge per carbon atom on the positive electrode for the three nanoporous carbon materials. At $t = 0$, the potential difference between the electrodes is suddenly switched from 0 to 1 V.

amount of charge stored depends on the rate of charging: For example, in nanopowders of CDCs, the specific capacitance was shown to decrease by 15−40% when the current density is switched from 0.1 to 5 A g^{-1} during galvanostatic cycling.[33] Our simulation setup corresponds to an instantaneous change of potential, so that we expect our results to match experimental ones in the limit of high current densities. Note that even if smaller than the equilibrium one, the final charge of the CDCs in the present simulations remains much larger than in the case of planar graphite electrodes, for which 0.004 e are stored per carbon atom for the same applied electric potential of 1 V.[34] The comparison of the different porous materials shows that CDC-1200 and CDC-950 seem to have similar charging profiles on Figure 2 while that of CDC-800 is markedly different: it takes a much longer time to reach the plateau régime for the latter. This behavior can be linked to the average pore sizes, which are identical for CDC-1200 and CDC-950, with those of CDC-800 being smaller.[30] We will now further analyze the dynamics on the local scale.

Charging Heterogeneity. In constant potential simulations, the charge carried by each carbon atom is calculated every time step. It is, thus, possible to examine the evolution of the local charge for any well-defined region of the electrode. To illustrate the charge penetration inside the electrode, Figure 3 displays the charging profiles as a function of depth (z, as defined on Figure 1) inside the positive electrodes for the three CDCs. The charge is calculated for the whole slab of carbon atoms with positions between $z - \delta$ and $z + \delta$ (δ = 0.5 Å here); it reflects the local imbalance in the number of cations and anions induced by the applied potential, which is strongly affected by the local topology and connectivity of the nanoporous material. The origin ($z = 0$) corresponds to the frontier between the electrolyte and the electrode. There is a general tendency for the charge to penetrate progressively from the boundary toward the interior of the

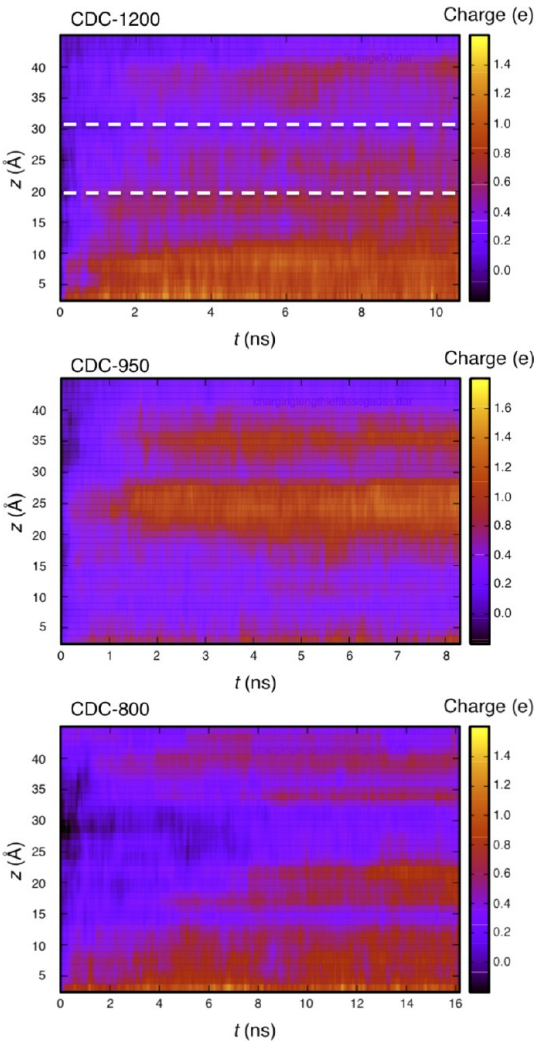

Figure 3. Evolution of the local charge with time as a function of depth (z, see Figure 1) inside the positive electrodes for the three CDCs. At each time step, the charge is calculated for the whole slab of carbon atoms with positions between $z - \delta$ and $z + \delta$ (δ = 0.5 Å here). Dark regions have a null charge, while yellow-colored ones have a high positive charge. The dashed lines on the top panel delimit the slice which is further analyzed on Figure 4.

electrode as the diffusive ion exchange process reaches greater depths. This is consistent with the transmission line models which are used for representing supercapacitors at the macroscopic scale as equivalent electric circuits,[35] and is in qualitative agreement with the results of Kondrat and Kornyshev, who showed by using a mean-field model that the charging of initially wetted single pores occurs by a diffusive ion exchange.[25] In the present case, the complex network of pores is initially wetted by the ionic liquid. The diffusive charging of the nanoporous carbon is, however, very heterogeneous at the nanometric scale, since some regions very deep inside the electrode start to charge relatively quickly after the electric potential is applied. For example, for CDC-950, there is a large increase of the charge in the middle of the electrode

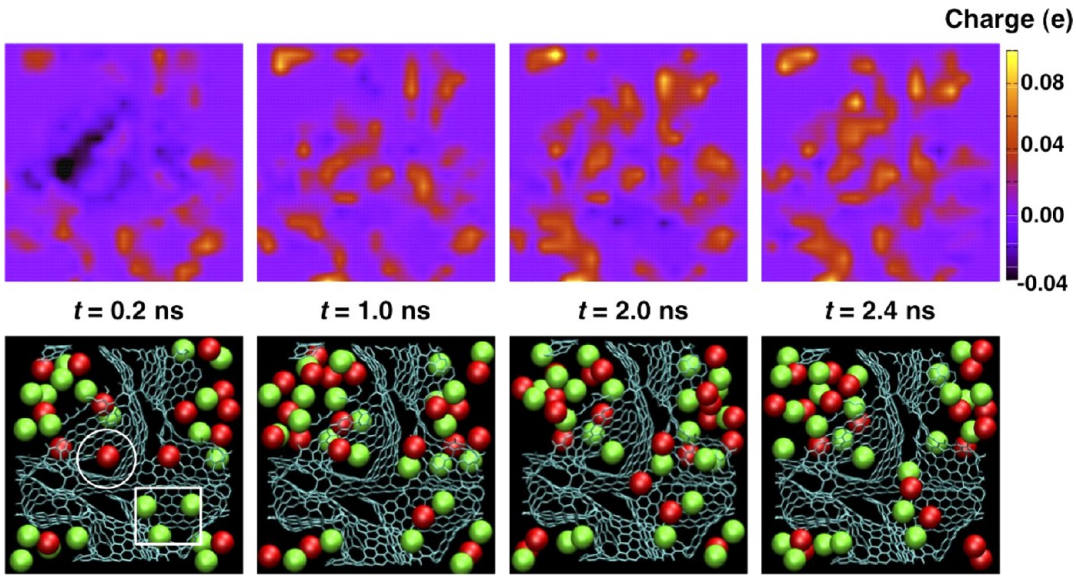

Figure 4. (Top) Repartition of the local charge inside a 11 Å-thick slice of the CDC-1200 positive electrode (corresponding to the zone with 19.5 Å < *z* < 30.5 Å which is delimited on Figure 3), for different times of simulation. (Bottom) Snapshots showing the electrode structure and the instantaneous ionic positions for this slice (red, cations centers of mass; green, anions) at the corresponding times. The white circle and square on the bottom left panel indicate regions which are discussed in the text.

for 1 ns < *t* < 2 ns. This is due to the presence of a large pore ending close to this region (see the snapshot provided in the Supporting Information), which acts as an electrolyte reservoir. Another indicator of this heterogeneity in charging can be seen in CDC-800, for which the region around *z* = 40 Å starts to charge long before the one at 35 Å.

To further illustrate the importance of the local structure on the heterogeneous charging, the rearrangement of the local charge inside a 11 Å-thick slice centered 25 Å away from the interface (*i.e.*, corresponding to 19.5 Å < *z* < 30.5 Å on Figure 3) is shown at various simulation times for the positive CDC-1200 electrode on Figure 4. The structure differs substantially from pictures based on regular, long pores such as carbon nanotubes. It is better described as a complex network of interconnected edge, planar, hollow or pocket sites of size barely larger than a few ionic radii, and the ions sample various adsorption modes.[36,37] The amount of charge which is stored locally increases with the degree of confinement of these sites.[38] A highly confined site close to the center of the slice is indicated with a white circle on Figure 4. At *t* = 0.2 ns, this site is occupied by a cation and the local charge on the electrode is negative. At *t* = 1.0 ns, there is an ion pair, and the cation is then expelled, resulting in the formation of a high positive charge on the carbon electrode. At the bottom right corner of the slice, a wider pore is present (it is indicated with a white square on Figure 4). It is already well charged at *t* = 0.2 ns, with 3 anions lying close to the surface. Subsequently, though, one of the anions leaves the pore for another region. It is replaced by a cation, decreasing the local charge. There is, therefore, an interplay between the various pores: their local charge increases on the nanosecond time scale but it is subject to fluctuations due to the diffusion of the ions inside the electrodes. In addition to the pore sizes, the connectivity between the pores should play an important role in the charging process and influence its heterogeneous character.

Equivalent Circuit. The interpretation of experiments on supercapacitors usually relies on the use of equivalent electric circuits. Here we examine the relevance of such macroscopic models in the light of our microscopic simulations and the implications of the latter for transport on larger scales. The most commonly used model in the case of nanoporous electrodes is that of a transmission line, in which the charge penetrates progressively into the electrode.[35,39] This model is based on an infinite succession of slices connected in parallel (*via* the constant potential solid surface), each of them consisting of a capacitor, accounting for the possibility to store charge locally *via* the polarization of the electrolyte at the surface of the pores, and of a resistance describing the dissipative electrolyte transport through the pores.

The link between such effective macroscopic models and the underlying microscopic mechanisms remains to be established. A key question, discussed below, is the definition of the equivalent circuit slices from the microscopic structure of the electrode, which should be as large as possible to ensure a good representation of the chosen regions. It should be large enough to ensure that the sum of all the heterogeneous charging events results in an homogeneous charging at the scale of the slice. Given the small size of the simulated system, we have thus divided each electrode into two slices of equal thickness *l*, resulting

TABLE 1. Parameters Employed in the Equivalent Circuit Models[a]

	CDC-1200	CDC-950	CDC-800
$R_{bulk}(10^8\Omega)$	1.0	1.1	1.2
$R_l(10^8\Omega)$	1.2	0.7	4.9
$C_1(10^{-18}F)$	4.3	3.6	3.9
$C_2(10^{-18}F)$	2.7	3.2	2.6

[a] In all cases, the bulk electrolyte region thickness is 50 Å for each half-cell, while the considered electrode slices have a $l = 21$ Å thickness.

in the equivalent electric circuit illustrated on Figure 1. R_{bulk} is the resistance of the electrolyte in the bulk region, R_l is the resistance of each electrode slice, C_1 and C_2 are the capacitances of the two slices. Among these quantities, the only unknown is R_l, which can be determined by fitting the total electrode charge evolution with time. It is given by

$$Q(t) = Q_{max}\left[1 - A_1\exp\left(-\frac{t}{\tau_1}\right) - A_2\exp\left(-\frac{t}{\tau_2}\right)\right] \quad (1)$$

where the expressions for Q_{max}, A_1, A_2, τ_1 and τ_2 are given as a function of the electric circuit components in the Supporting Information. The fitting was made on the bulk part of the electrode, *i.e.*, by excluding the first 5 Å of the electrode in order to avoid interfacial effects. Note that including this region, although decreasing the quality of the fit, does not change the results qualitatively.

The values of all the calculated and fitted parameters are given in Table 1 (see the Supporting Information for additional details), and results of the fits are shown on Figure 5 for the three CDC electrodes. In all cases eq 1 underestimates the charge at short times but the matching is very good for intermediate and long times. To check the transferability of this approach, we have made two different tests. First we have calculated the charges in the two slices (expressions provided in the Supporting Information); they correspond very well with the data extracted from the simulations, without further parameter fitting. Second, we have compared the charging dynamics for an applied potential of 2 V with the prediction from eq 1 using the R_l values fitted at 1 V. Again, a good agreement was obtained (the data is shown on Supplementary Figure 4). Therefore the proposed equivalent circuit is clearly able to capture the charging behavior of our modeled supercapacitor. Given the relative widths of the electrolyte (50 Å for each half-cell) and electrode regions ($2l$ = 42 Å for each electrode) in our simulation cells, we can conclude from the fact that R_{bulk} is of the same order of magnitude as R_l for both CDC-1200 and CDC-950 that the transport of the ions is only slightly affected inside the pores. This is consistent with the structure of these

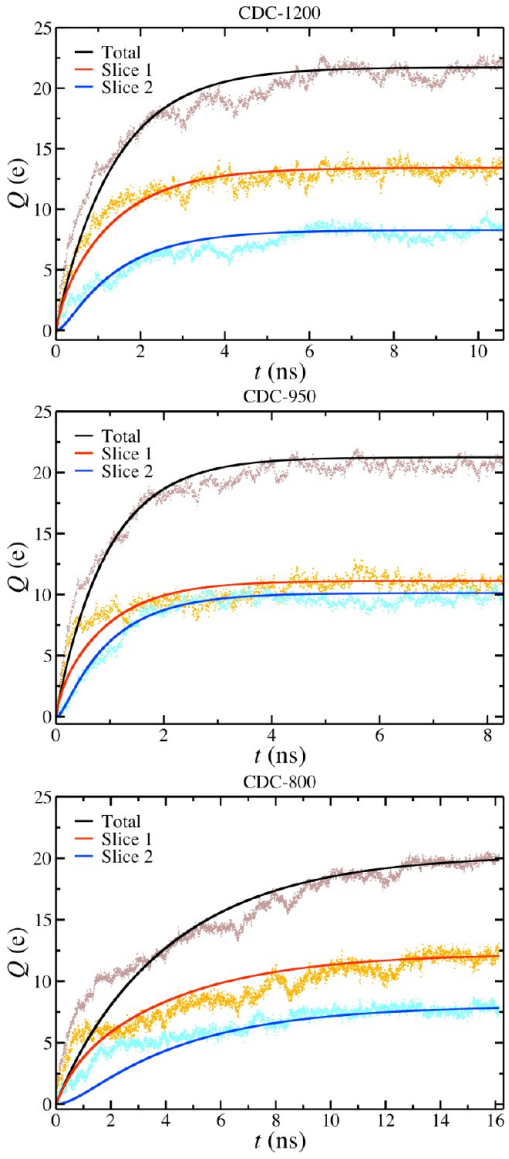

Figure 5. Total charge of the electrodes as a function of time for the three systems. Molecular dynamics simulation results are well described by eq 1, which corresponds to the equivalent circuit displayed on Figure 1, with the parameters of Table 1. The only parameter adjusted to reproduce these results is the resistance of the electrode slices, R_l. The charge of each slice predicted with the equivalent circuit is also in good agreement with the simulation data, without further parameter fitting.

electrodes, which contain interconnected nanopores with an average pore size of 9.0 Å. For CDC-800, the transport inside the smaller pores is slower, by a factor of approximately 4−8. The low resistivity of the electrolyte inside the electrodes may arise from the existence of collective transport effects, as suggested by a recent study from Kondrat *et al.* in which the diffusion coefficients of the ions from an ionic liquid adsorbed inside electrified slit pores were shown to be strongly dependent on the charged state of the electrode.[40]

Charging on Larger Scales. The good agreement between the simple two-slice model and the molecular

simulation results further indicates that the size of the regions defining the slices is adequate. More precisely, this length scale is sufficiently large to average out some of the local heterogeneity of the charging process, while allowing the diffusive behavior to be captured on a coarser scale. Identifying the relevant length scales for the definition of coarse-grained ionic and charge densities might also be useful in the framework of mesoscopic models such as time-dependent Density Functional Theory.[25] In addition, we can also extract from this effective macroscopic model a crude estimate of the characteristic charging time constant, which would probably need to be improved by using larger simulation cells. In the full transmission line model, the diffusive charging occurs over the thickness l_{macro} of the electrodes with a characteristic time scale RCl^2_{macro}, with R and C the resistance and capacitance *per unit length*, respectively. This time can be determined from our simulation results as

$$\tau(l_{macro}) = R_l \times C_{tot} \times \left(\frac{l_{macro}}{l_{sim}}\right)^2 \qquad (2)$$

where C_{tot} is given by the total capacitance of the electrodes and l_{sim} their thickness in our simulations. For a typical commercial supercapacitor, the electrode size is $l_{macro} \sim 100\ \mu$m, which gives us characteristic charging times ranging between 0.5 and 4 s for our systems, in good agreement with the experimental data: for example, in reference 11, relaxation time constants, defined as the minimum time needed to discharge all the energy from the supercapacitor cell with an efficiency greater than 50%, of 5−20 s were measured with similar CDCs to the ones we simulate (although the electrolyte is different, its electrical conductivity is of the same order of magnitude as the ionic liquid in the present study, and so would be the corresponding R_{bulk}). Our estimate does not take into account the thickness of the electrolyte region and the resistance of other components of the supercapacitor such as the separator, but these should not impact the charging time significantly.

CONCLUSION

In conclusion, we have used molecular dynamics simulations in order to study the charging of electrified nanoporous CDC electrodes impregnated with a BMI-PF_6 electrolyte. We have shown that it occurs in a diffusive way, in agreement with the recent literature.[25] The charge starts from the electrode/electrolyte interface and penetrates progressively into the bulk of the carbon material. At the nanometer scale, though, strong heterogeneities are observed due to the particular structure of CDCs. These materials consist in a complex network of pores of various sizes, and differ substantially from the carbon nanotubes or the slit pores which are often used to model them. Depending on the local organization of the porous networks, some regions may start to charge before others despite being located more deeply inside the electrode. For example, in CDC-950, a region in the middle of the electrode charges very quickly because it is located near to a large pore of the carbon.

By comparing three CDCs with different structures, we have shown that the charging time depends on the average pore size. CDC-1200 and CDC-950, which have similar average pore sizes, are charged on similar time scales, even though the details of the pore connectivity and the distribution of pore throats may also play a role. The process is slower by a factor of 4−8 in the case of CDC-800, which has a smaller average pore size. Experimental supercapacitors involving nanoporous carbon show good power performances in addition to their excellent energy densities,[11] a result which seemed rather counterintuitive and had not been explained at the microscopic scale previously. From our molecular dynamics simulations data, we have fitted a macroscopic model based on an equivalent electric circuit. The transmission line model which is used in experiments is clearly able to capture the charging behavior. This fit provides us with a value for the resistance of the electrolyte inside the pores. This quantity is of the same order of magnitude as that of the bulk electrolyte (for similar dimensions), which leads to charging times of one to ten seconds time scale for a 100 μm thick electrode. This confirms that the transport of the ions is not much affected in the porous materials. In future work we will investigate whether the fast charging that we observe can be associated with the existence of collective transport effects, as suggested by the recent work from Kondrat *et al.*[40] If the existence of such a mechanism leading to fast transport of the charge is shown to be universal for a series of electrolytes and electrode structures, it means that nanoporous-carbon based supercapacitors have inherently high power densities, so that the quest for new carbon materials should mainly focus on enhancing their energy density.

METHODS

The simulation cells consists of [BMI][PF_6] ionic liquid (600 ion pairs) surrounded by two identical and symmetric nanoporous carbon electrodes, obtained by quenched molecular dynamics.[30] Following our previous works, we use for the ionic liquid the coarse-grained model of Roy and Maroncelli, which yields the correct structural, thermodynamic and dynamic properties of BMI-PF_6.[41] Three and one sites describe the cation and the anion, respectively.[34,42] The sizes of the simulation cells are chosen in order to reproduce the experimental densities of the bulk electrolyte. Supporting Information Table 1 gathers the number of carbon atoms and the lengths for all the simulation cells for each type of studied carbon.

Molecular dynamics simulations are conducted on the three different systems, with a time step of 2 fs which is consistent with the coarse-grained model used. The forces are calculated as the sum of site−site Lennard-Jones potential and Coulombic interactions. Parameters for the ions and carbon atoms are the same as in our previous work.[18,34,42] In all the simulations, the Coulomb interactions are calculated through a two-dimensional Ewald summation.[43,44]

The procedure to simulate the charging process follows two steps: the system is first equilibrated for a few nanoseconds, first with a constant charge of 0 e on all carbon atoms and then with a 0 V potential difference between the two electrodes. At $t = 0$, this potential difference $\Delta\psi^0$ is suddenly set to 1 V ($\psi^+ = 0.5$ V and $\psi^- = -0.5$ V or 2 V. The electrodes are held at constant potential using a method developed by Reed *et al.*[43] from an original proposal by Siepmann.[45] Simulations are continued for sufficiently long to reach equilibrium, *i.e.*, to exhibit a long plateau for the value of the charge on carbon atoms. The constant potential approach is computationally expensive compared to the constant charge approach but is essential to study realistically dynamic processes such as the charging process.[38] Typically, 50 000 CPU hours were needed to gather a trajectory of 1 ns for a given system.

Controlling the temperature is an important concern for such simulations. In a macroscopic experiment, the supercapacitor is thermostated in order to control its temperature. It is therefore preferable to simulate the systems in the *NVT* ensemble, keeping a weak coupling to the heat-bath in order to avoid the dynamics being dictated by the thermostat relaxation time. Here we have used a Nosé-Hoover thermostat[46] with a relaxation time of 10 ps and a target temperature of 400 K. The variations of temperature with time are shown in the Supporting Information for $\Delta\psi^0 = 1$ V: the largest increase is observed in the case of CDC-1200, for which the temperature switches from 400 to 470 K during the first nanosecond due to the Joule heating effect,[29] then up to 490 K during the next 5 ns before starting to decrease slightly. The diffusion coefficients increase by a factor of 2−3 in this temperature range in the bulk ionic liquid,[41] which has to be taken into account when analyzing the results. The increase of temperature is larger for the two other applied potentials; all the results presented here, therefore, correspond to the 1 V case, although the charging dynamics is qualitatively the same for $\Delta\psi^0 = 2$ V.

Conflict of Interest: The authors declare no competing financial interest.

Acknowledgment. We acknowledge the support of the French Agence Nationale de la Recherche (ANR) under grant ANR-2010-BLAN-0933-02 ('Modeling the Ion Adsorption in Carbon Micropores'). The research leading to these results has received funding from the European Research Council under the European Union's Seventh Framework Programme (FP/2007-2013)/ERC Grant Agreement n. 102539. We are grateful for the computing resources on JADE (CINES, French National HPC) obtained through the project c2013096728. We acknowledge PRACE for awarding us access to resource CURIE based in France at TGCC.

Supporting Information Available: Additional computational details, variation of temperature due to Joule effect, details of the equivalent circuit modeling and charging dynamics for an applied potential of 2 V. This material is available free of charge *via* the Internet at http://pubs.acs.org.

REFERENCES AND NOTES

1. Miller, J. R.; Simon, P. Electrochemical Capacitors for Energy Management. *Science* **2008**, *321*, 651–652.
2. Simon, P.; Gogotsi, Y. Materials for Electrochemical Capacitors. *Nat. Mater.* **2008**, *7*, 845–854.
3. Frackowiak, E.; Abbas, Q.; Béguin, F. Carbon/Carbon Supercapacitors. *J. Energy Chem.* **2013**, *22*, 226–240.
4. Armand, M.; Tarascon, J.-M. Building Better Batteries. *Nature* **2008**, *451*, 652–657.
5. Chen, L.-F.; Zhang, X.-D.; Liang, H.-W.; Kong, M.; Guan, Q.-F.; Chen, P.; Wu, Z.-Y.; Yu, S.-H. Synthesis of Nitrogen-Doped Porous Carbon Nanofibers as an Efficient Electrode Material for Supercapacitors. *ACS Nano* **2012**, *6*, 7092–7102.
6. Wu, Z.-S.; Sun, Y.; Tan, Y.-Z.; Yang, S.; Feng, X.; Mullen, K. Three-Dimensional Graphene-Based Macro- and Mesoporous Frameworks for High Performance Electrochemical Capacitive Energy Storage. *J. Am. Chem. Soc.* **2012**, *134*, 19532–19535.
7. Wu, Z.-S.; Parvez, K.; Feng, X.; Müllen, K. Graphene-Based In-Plane Micro-Supercapacitors with High Power and Energy Densities. *Nat. Commun.* **2013**, *4*, 2487.
8. Hao, G.-P.; Lu, A.-H.; Dong, W.; Jin, Z.-Y.; Zhang, X.-Q.; Zhang, J.-T.; Li, W.-C. Sandwich-Type Microporous Carbon Nanosheets for Enhanced Supercapacitor Performance. *Adv. Energy Mater.* **2013**, *3*, 1421–1427.
9. Yang, X.; Cheng, C.; Wang, Y.; Qiu, L.; Li, D. Liquid-Mediated Dense Integration of Graphene Materials for Compact Capacitive Energy Storage. *Science* **2013**, *341*, 534–537.
10. DeBlase, C. R.; Silberstein, K. E.; Truong, T.-T.; Abruna, H. D.; Dichtel, W. R. β-Ketoenamine-Linked Covalent Organic Frameworks Capable of Pseudocapacitive Energy Storage. *J. Am. Chem. Soc.* **2013**, *135*, 16821–16824.
11. Chmiola, J.; Yushin, G.; Gogotsi, Y.; Portet, C.; Simon, P.; Taberna, P. L. Anomalous Increase in Carbon Capacitance at Pore Sizes Less Than 1 Nanometer. *Science* **2006**, *313*, 1760–1763.
12. Raymundo-Piñero, E.; Kierzek, K.; Machnikowski, J.; Béguin, F. Relationship between the Nanoporous Texture of Activated Carbons and their Capacitance Properties in Different Electrolytes. *Carbon* **2006**, *44*, 2498–2507.
13. Largeot, C.; Portet, C.; Chmiola, J.; Taberna, P. L.; Gogotsi, Y.; Simon, P. Relation Between the Ion Size and Pore Size for an Electric Double-Layer Capacitor. *J. Am. Chem. Soc.* **2008**, *130*, 2730–2731.
14. Wu, P.; Huang, J. S.; Meunier, V.; Sumpter, B. G.; Qiao, R. Complex Capacitance Scaling in Ionic Liquids-Filled Nanopores. *ACS Nano* **2011**, *5*, 9044–9051.
15. Shim, Y.; Kim, H. J. Nanoporous Carbon Supercapacitors in an Ionic Liquid: A Computer Simulation Study. *ACS Nano* **2010**, *4*, 2345–2355.
16. Kondrat, S.; Kornyshev, A. A. Superionic State in Double-Layer Capacitors with Nanoporous Electrodes. *J. Phys.: Condens. Matter* **2011**, *23*, 022201.
17. Kondrat, S.; Perez, C. R.; Presser, V.; Gogotsi, Y.; Kornyshev, A. A. Effect of Pore Size and its Dispersity on the Energy Storage in Nanoporous Supercapacitors. *Energy Environ. Sci.* **2012**, *5*, 6474–6479.
18. Merlet, C.; Rotenberg, B.; Madden, P. A.; Taberna, P.-L.; Simon, P.; Gogotsi, Y.; Salanne, M. On the Molecular Origin of Supercapacitance in Nanoporous Carbon Electrodes. *Nat. Mater.* **2012**, *11*, 306–310.
19. Wu, P.; Huang, J.; Meunier, V.; Sumpter, B. G.; Qiao, R. Voltage Dependent Charge Storage Modes and Capacity in Sub-Nanometer Pores. *J. Phys. Chem. Lett.* **2012**, *3*, 1732–1737.
20. Xing, L.; Vatamanu, J.; Borodin, O.; Bedrov, D. On the Atomistic Nature of Capacitance Enhancement Generated by Ionic Liquid Electrolyte Confined in Subnanometer Pores. *J. Phys. Chem. Lett.* **2013**, *4*, 132–140.
21. Feng, G.; Li, S.; Presser, V.; Cummings, P. T. Molecular Insights into Carbon Supercapacitors Based on Room Temperature Ionic Liquids. *J. Phys. Chem. Lett.* **2013**, *4*, 3367–3376.
22. Lanning, O.; Madden, P. A. Screening at a Charged Surface by a Molten Salt. *J. Phys. Chem. B* **2004**, *108*, 11069–11072.
23. Pinilla, C.; Del Pópolo, M. G.; Kohanoff, J.; Lynden-Bell, R. M. Polarization Relaxation in an Ionic Liquid Confined between Electrified Walls. *J. Phys. Chem. B* **2007**, *111*, 4877–4884.
24. Vatamanu, J.; Borodin, O.; Smith, G. D. Molecular Simulations of the Electric Double Layer Structure, Differential Capacitance, and Charging Kinetics for *N*-Methyl-*N*-propylpyrrolidinium Bis(fluorosulfonyl)imide at Graphite Electrodes. *J. Phys. Chem. B* **2011**, *115*, 3073–3084.
25. Kondrat, S.; Kornyshev, A. A. Charging Dynamics and Optimization of Nano-Porous Supercapacitors. *J. Phys. Chem. C* **2013**, *117*, 12399–12406.

26. Reed, S. K.; Madden, P. A.; Papadopoulos, A. Electrochemical Charge Transfer at a Metallic Electrode: A Simulation Study. *J. Chem. Phys.* **2008**, *128*, 124701.
27. Vatamanu, J.; Borodin, O.; Smith, G. D. Molecular Insights into the Potential and Temperature Dependences of the Differential Capacitance of a Room-Temperature Ionic Liquid at Graphite Electrodes. *J. Am. Chem. Soc.* **2010**, *132*, 14825–14833.
28. Merlet, C.; Rotenberg, B.; Madden, P. A.; Salanne, M. Computer Simulations of Ionic Liquids at Electrochemical Interfaces. *Phys. Chem. Chem. Phys.* **2013**, *15*, 15781–15792.
29. Merlet, C.; Péan, C.; Rotenberg, B.; Madden, P. A.; Simon, P.; Salanne, M. Simulating Supercapacitors: Can We Model Electrodes as Constant Charge Surfaces? *J. Phys. Chem. Lett.* **2013**, *4*, 264–268.
30. Palmer, J. C.; Llobet, A.; Yeon, S.-H.; Fisher, J. E.; Shi, Y.; Gogotsi, Y.; Gubbins, K. E. Modeling the Structural Evolution of Carbide-Derived Carbons Using Quenched Molecular Dynamics. *Carbon* **2010**, *48*, 1116–1123.
31. Gogotsi, Y.; Nikitin, A.; Ye, H.; Zhou, W.; Fischer, J. E.; Yi, B.; Foley, H. C.; Barsoum, M. W. Nanoporous Carbide-Derived Carbon with Tunable Pore Size. *Nat. Mater.* **2003**, *2*, 591–594.
32. Kondrat, S.; Georgi, N.; Fedorov, M. V.; Kornyshev, A. A. A Superionic State in Nano-Porous Double-Layer Capacitors: Insights from Monte Carlo Simulations. *Phys. Chem. Chem. Phys.* **2011**, *13*, 11359–11366.
33. Perez, C. R.; Yeon, S.-H.; Segalini, J.; Presser, V.; Taberna, P.-L.; Simon, P.; Gogotsi, Y. Structure and Electrochemical Performance of Carbide-Derived Carbon Nanopowders. *Adv. Funct. Mater.* **2013**, *23*, 1081–1089.
34. Merlet, C.; Salanne, M.; Rotenberg, B.; Madden, P. A. Imidazolium Ionic Liquid Interfaces with Vapor and Graphite: Interfacial Tension and Capacitance from Coarse-Grained Molecular Simulations. *J. Phys. Chem. C* **2011**, *115*, 16613–16618.
35. Conway, B. E. *Electrochemical Supercapacitors: Scientific Fundamentals and Technological Applications*; Kluwer: New York, 1999.
36. Wang, H.; Koster, T. K. J.; Trease, N. M.; Segalini, J.; Taberna, P. L.; Simon, P.; Gogotsi, Y.; Grey, C. P.; Real-Time, N. M. R. Studies of Electrochemical Double-Layer Capacitors. *J. Am. Chem. Soc.* **2011**, *133*, 19270–19273.
37. Deschamps, M.; Gilbert, E.; Azais, P.; Raymundo-Piñero, E.; Ammar, M. R.; Simon, P.; Massiot, D.; Béguin, F. Exploring Electrolyte Organization in Supercapacitor Electrodes with Solid-State NMR. *Nat. Mater.* **2013**, *12*, 351–358.
38. Merlet, C.; Péan, C.; Rotenberg, B.; Madden, P. A.; Daffos, B.; Taberna, P.-L.; Simon, P.; Salanne, M. Highly Confined Ions Store Charge More Efficiently in Supercapacitors. *Nat. Commun.* **2013**, *4*, 2701.
39. Taberna, P.-L.; Simon, P.; Fauvarque, J.-F. Electrochemical Characteristics and Impedance Spectroscopy Studies of Carbon-Carbon Supercapacitors. *J. Electrochem. Soc.* **2003**, *150*, A292–A300.
40. Kondrat, S.; Wu, P.; Qiao, R.; Kornyshev, A. Accelerating Charging Dynamics in Sub-Nanometer Pores. *arXiv* **2013**, No. 1311.7529.
41. Roy, D.; Maroncelli, M. An Improved Four-Site Ionic Liquid Model. *J. Phys. Chem. B* **2010**, *114*, 12629–12631.
42. Merlet, C.; Salanne, M.; Rotenberg, B. New Coarse-Grained Models of Imidazolium Ionic Liquids for Bulk and Interfacial Molecular Simulations. *J. Phys. Chem. C* **2012**, *116*, 7687–7693.
43. Reed, S. K.; Lanning, O. J.; Madden, P. A. Electrochemical Interface Between an Ionic Liquid and a Model Metallic Electrode. *J. Chem. Phys.* **2007**, *126*, 084704.
44. Gingrich, T. R.; Wilson, M. On the Ewald Summation of Gaussian Charges for the Simulation of Metallic Surfaces. *Chem. Phys. Lett.* **2010**, *500*, 178–183.
45. Siepmann, J. I.; Sprik, M. Influence of Surface-Topology and Electrostatic Potential on Water Electrode Systems. *J. Chem. Phys.* **1995**, *102*, 511–524.
46. Nosé, S. A Unified Formulation of the Constant Temperature Molecular Dynamics Methods. *J. Chem. Phys.* **1984**, *81*, 511–519.